第 36 卷 第 3 期
2021 年 6 月

新 型 炭 材 料
NEW CARBON MATERIALS

Vol. 36　No. 3
Jun. 2021

Near-infrared emission carbon dots for bio-imaging applications

LI Li-ping[1,2],　　REN Xiao-feng[1],　　BAI Pei-rong[2],　　LIU Yan[2],　　XU Wei-yue[2],

XIE Jun[1,*],　　ZHANG Rui-ping[2,*]

(1. *School of Basic Medical Science*, *Shanxi Medical University*, *Taiyuan* 030001, *China*;

2. *Third Hospital of Shanxi Medical University*, *Shanxi Bethune Hospital*, *Shanxi Academy of Medical Sciences*, *Taiyuan* 030032, *China*)

Abstract：　　It is very difficult to prepare red/near-infrared emission carbon dots (CDs) for bio-imaging applications which are needed because of their deep tissue penetration, minimal auto-fluorescence, and low emission light damage to bio-tissues. Near-infrared emitting CDs (NIR-CDs) were synthesized from sulfonated tetraphenylporphyrin using a solvothermal method. They have excitation-independent properties with a maximum emission at 692 nm. Studies showed that this unique near-infrared emission mainly originated from the aggregated molecular states of the CDs. The NIR-CDs showed good water solubility, exceptional biocompatibility, low toxicity, and superior cellular labelling ability. This work could significantly advance the structural design and preparation of NIR-CDs and corresponding bio-imaging applications.

Key words: Near-infrared emission；Molecular states；Cellular labelling；Bio-imaging

1　Introduction

Carbon dots (CDs), as a novel carbon-based zero-dimensional nanomaterial, have drawn merits owing to their low toxicity, tunable emission, excellent water solubility, great biocompatibility, numerous functional abilities and low cost[1–3]. In the meantime, CDs are uncomplicated to be fabricated via hydrothermal treatments[4], laser ablation[5], microwave-assisted method[6], and electrochemical oxidation[7] with various precursors, including natural products[8], chemical agents[9], biomaterials[10], and so on. Given that, CDs display wide range of potential applications in various fields, particularly in biomedical fields, such as biolabelling[11], bioimaging[12], biosensing[13], and drug delivery[14]. Nevertheless, most of the reported CDs retain blue or green light emission, which harshly hinders their optical applications in biology due to the strong tissue absorption, shallow tissue penetration, and high interference from the biological system's autofluorescence or severe photodamage[15]. Consequently, it is imperative to develop effective red/near-infrared (R/NIR) emitting CDs, which are more appropriate alternates for photobleaching-prone organic dyes and toxic semiconductors quantum dots.

To date, only few groups have efficaciously synthesized R-CDs, and the emission wavelengths are primarily below 650 nm[16–18]. Yang's group reported that the electrochemically exfoliated graphite formed R-CDs with an emission wavelength at 610 nm[19]. At the same time, Lu's group obtained R-CDs by solvothermal treatment of citric acid and thiourea in dimethylformamide, and the optimal emission was located at 610 nm with QYs of 24%[16]. Lin's group produced brighter R-CDs (QYs was higher to 28%) from precursors with π-conjugated structure (i.e. p-phenylenediamine), and the maximum emission peak was at 603 nm[20]. It remains urgent to develop near-infrared fluorescent CDs (NIR-CDs) with fluorescence emission wavelengths longer than 650 nm.

Although the luminescence mechanism of CDs is not fully understood, it is commonly accepted that the luminescence is generated from carbogenic core state, surface state and molecule fluorescence[21]. These origins and corresponding mechanisms are commonly used to explain and guide the design of NIR-CDs. In our earlier work, the NIR-CDs were synthesized from spinach via a one-step solvothermal treatment, and the maximum fluorescence emission wavelength is up to

680 nm, longer than most reported NIR-CDs[22]. The luminescence of NIR-CDs is thought to originate from the electron transition of multiple emission centers, including molecular states and carbon-core states. Lin's group has synthesized NIR-CDs (λ_{max} = 683 nm) for two-photon fluorescence bioimaging, and the emission is mainly from the molecular state mechanism[23].

Motivated by the pioneering and our previous works, we devised and produced NIR-CDs using sulfonated tetraphenylporphyrin as a precursor through a solvothermal treatment. The NIR-CDs present excitation-independent properties with a maximum emission at 692 nm. Further studies revealed that the NIR fluorescence properties mainly originated from the aggregated molecular states of CDs. Besides, the as-obtained NIR-CDs also revealed good water solubility, exceptional compatibility, ignorable toxicity, and superb cellular labelling capability. Given that their collective properties, the NIR-CDs as effective near-infrared emission bio-imaging probes with ignorable toxicity hold great potential for *in vitro* and *in vivo* imaging in the future.

2　Materials and methods

2.1　Chemicals

Tetraphenylporphyrin was purchased from Sinopharm. Dulbecco's Modified Eagle Medium (DMEM), penicillin, streptomycin, and fetal bovine serum (FBS) were purchased from Gibco. Phosphate buffered saline (PBS), culture dishes, 96-well plates, and confocal dishes were purchased from Taiyuan Zhenghe Biochemical Reagent Company. 3-(4, 5-dimethyl-2-thiazolyl)-2, 5-diphenyltetrazolium bromide (MTT) was obtained from Sigma Aldrich Corporation. Concentrated sulfuric acid (98%) and hydrochloric acid were obtained from Sinopharm Group Chemical Reagent Corporation. The above chemicals and solvents were of reagent grade and used as received. Filtration membranes (0.1 μm) and dialysis membranes (MWCD= 3 500) were purchased from Spectrum Labs, China. HeLa cells were purchased from Tongpai (Shanghai) Biotechnology Corporation.

2.2　Synthesis of NIR-CDs

First, the tetraphenylporphyrin was diffused in concentrated sulfuric acid and then treated with salting-out precipitation, neutralisation, and methanol precipitation to obtain sulfonated tetraphenylporphyrin. Then the above solution was dispersed in hydrochloric acid and transferred into a Teflon-lined autoclave, pursued by solvothermal treatment at 180 °C for 6 h. Following cooling to room temperature, the acquired NIR-CDs solution was filtered by 0.1 μm filter membrane, then dialyzed with a dialysis membrane (a cutting molecular weight of 3 500) for three days. The unreacted raw materials and small molecular weight products were entirely removed, and the objective product NIR-CDs solution was obtained. Ultimately, the NIR-CDs solution was freeze-dried to obtain the NIR-CDs powder.

2.3　Characterization

The NIR-CDs' morphology and size were determined by transmission electron microscopy (TEM, JEM-2100F, JEOL, Japan) with an accelerating voltage of 200 kV. TEM samples were prepared by dispersing CDs in ethanol solution and then dropped on a copper mesh. The zeta potential of NIR-CDs was determined by a Zetasizer 3000 HS (Malvern, UK). The chemical structure and the NIR-CDs' elemental composition were characterized by X-ray photoelectron spectroscopy (XPS) and Fourier transform infrared spectrometer (FTIR). XPS was completed using an XPS spectrometer (Model: Thermo ESCALAB 250) with X-ray radiation of Al Kα (hυ = 1486.6 eV). FT-IR was characterized by an IR spectrometer (Model: Nicolet Magna-IR 550-II) in transmission mode using KBr pellets. The electron transitions and luminescence properties of NIR-CDs were characterized by UV-visible absorption spectroscopy and photoluminescence spectroscopy, respectively. The UV-visible absorption spectroscopy was collected by a UV-vis-NIR spectrophotometer (Model: Shimadzu UV-3600) at room temperature with a 1 cm quartz cuvette. The PL spectra were recorded on a FL spectrophotometer (Model: Hitachi F-7000). The cytotoxicity of NIR-CDs was detected by standard MTT assay and recor-

ded by a plate reader (Model: Tecan Infinite M1000). The cellulars were imaged on a laser scanning confocal microscope (Model: Nikon C1Si).

2.4　Cytotoxicity assay

Hela cells were propagated in DMEM medium supported with 10% FBS and 1% penicillin/streptomycin at 37 ℃ in a humidified incubator containing 5% CO_2. The standard MTT assay was used to evaluate the cytotoxicity of Hela cells labeled with NIR-CDs. The Hela cells were trypsinized and plated in a 96-well plate at a density of 10^4 cells/well, and allowed to adhere overnight. After being isothermally incubated for 24 h, the culture medium was substituted by fresh DMEM containing various concentrations of the NIR-CDs (0−400 μg mL^{-1}) for another 24 h followed by the standard MTT assay to measure the cell viability. Finally, each well's absorbance was measured on a Tecan Infinite M1000 plate reader at a wavelength of 570 nm. Measurements were repeated at least three times.

2.5　Cell imaging

HeLa cells were seeded at a density of 10^4 cells per well in confocal culture plates in DMEM culture medium. NIR-CD dispersion with the final concentration of 200 mg mL^{-1} was added to Hela cells for 1 h incubation. Then, the non-specifically bound NIR-CDs in the confocal culture plates were removed by PBS washing. Finally, the fluorescence images of the Hela cells were recorded at 100 ms intervals for each colour automatically by a NIS-element AR (Ver: 4.13.00) equipped with a water-cooled CCD camera.

3　Results and discussion

3.1　Characterization of NIR-CDs

The NIR-CDs were synthesized via a solvothermal method using sulfonated tetraphenylporphyrin as the precursor at 180 ℃ for 6 h, as shown in Fig. 1. The as-prepared NIR-CDs show good water solubility. The TEM images were listed in Fig. 2a, showing that the NIR-CDs have a uniform particle size distribution with an average of ～2.3 nm. The NIR-CDs have a diameter in the range of 1.5−3.5 nm (Fig. 2b). Fig. 2c presents the high-resolution TEM

image of NIR-CDs. The High-resolution TEM (HRTEM) images show that most of the NIR-CDs have a low carbonization degree, except for a small number of particles that are partially graphitized. The lattice fringe in Fig. 2d shows a space of 0.21 nm attributing to the (100) plane of graphite[24]. The XRD was also used to characterize the structure of NIR-CDs, as shown in Fig. S1. The diffraction peaks located at 23.7° and 44° are in close agreement with the (002) and (100) planes of carbon nanomaterials with a graphite-like structure[25, 26]. The broadening nature of the peak indicates a short-range ordered structure[1].

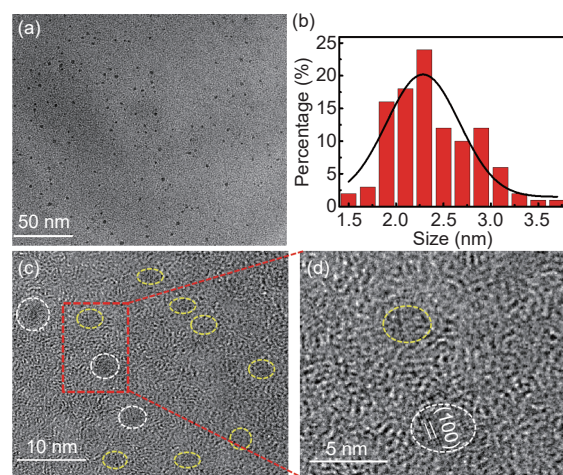Fig. 1　Synthetic route of NIR-CDs.

Fig. 2　(a) TEM and (b) the size distribution histogram of the NIR-CDs; (c, d) HRTEM images of the NIR-CDs. The white circles stand for crystalline NIR-CDs, and yellow circles represent amorphous CDs.

The NIR-CDs' elemental composition, chemical structures, and the surface functionalization were examined by XPS and FT-IR. Fig. 3 shows that NIR-CDs mainly contain carbon, nitrogen, oxygen and sulfur elements. The high-resolution XPS peak of C1s can be deconvoluted into four fitting peaks at 284.7, 285.4, 286.6 and 288.0 eV, corresponding to the C＝C/C—C, C—N, C—O and C＝N/C＝O species, respectively[27, 28]. The high-resolution XPS peak of N 1s of the NIR-CDs could be split into two peaks
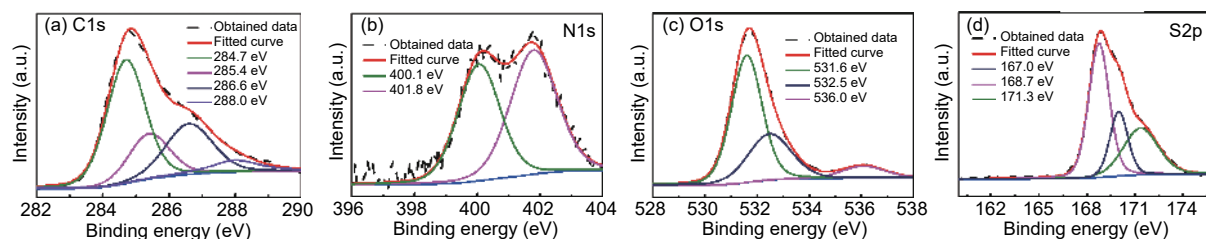
Fig. 3　(a-d) High-resolution scan of the C1s, N1s, O1s and S2p of the NIR-CDs.

centered at 400.1 and 400.8 eV, which are probably attributed to pyrrolic N and pyridinic N, respectively (Fig. 3b)[29, 30]. For the XPS peak of O1s (Fig. 3c), there are three fitting peaks at 531.6, 532.5 and 536.0 eV correspond to C=O, C—OH/C—O—C, and O=C—OH, respectively[15, 31, 32]. The XPS peak of S2p shows three fitting peaks at 168.7, 170.0, 171.3 eV (Fig. 3d). The peak at 168.7 eV agrees to the —C—SO$_3$ structure and the peaks at 170.0 and 171.3 eV relate to the S2$_{p1/2}$ and S2$_{p3/2}$ of the -SO$_4$ group of the NIR-CDs[33, 34].

　　To further investigate the surface groups of NIR-CDs, the FTIR spectrum was recorded. The peak centered at 3 448 cm^{-1} suggests the presence of O—H and N—H bonds on the surface of NIR-CDs[15]. The peaks at about 2 931, 1 645, 1 386, 1 070 cm^{-1} are assigned to the stretching vibrations of C—H stretching vibrations, C=C/C=O, —CH$_3$/=C—N, and C—O/—SO$_3$, respectively[35, 36]. The XPS and FTIR analysis corroborated that the NIR-CDs are doped by nitrogen and sulfur, and functional groups such as carboxyl, hydroxyl, amino, ester, and sulfonic groups coexist on the NIR-CDs surface. As shown in Fig. 4b, the zeta potential is −18.9 mV for the NIR-CDs dispersed in an aqueous solution, and the low potential results from the abundant carboxyl, hydroxyl, and sulfonic groups on the surface of NIR-CDs. The presence of hydrophilic groups promotes the dispersibility of NIR-CDs in water.

3.2　Optical properties of NIR-CDs

　　The UV-visible absorption and fluorescence excitation and emission of the NIR-CDs were examined to evaluate their optical properties. Fig. 5 shows four absorption peaks at 240, 344, 435 and 647 nm. The peak at 240 nm is typical π–π* transition of the aromatic sp^2 domain of nano-carbon as reported for most CDs[37, 38]. The absorbance peaks at 344, 435 and
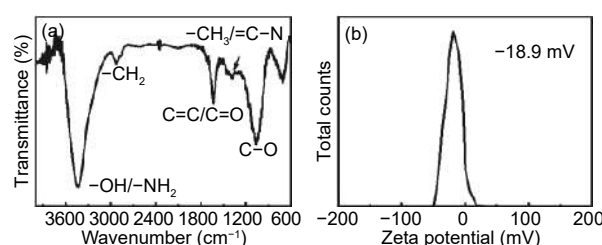

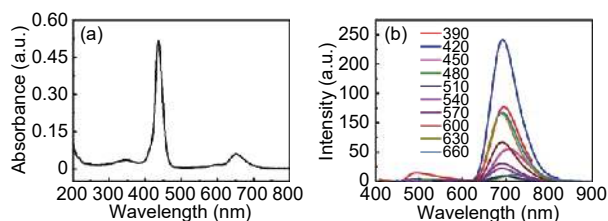Fig. 4　(a) FTIR spectrum and (b) Zeta potential of the NIR-CDs.

Fig. 5　(a) UV-visible absorption and (b) PL emission spectra of the NIR-CDs.

647 nm are possibly ascribed to the n–π* transitions of C=O, C=N, and C—S bonds in the sulfonated porphyrin structures, respectively[39, 40]. The PL spectra of the NIR-CDs measured at different excitation wavelengths present an excitation-independent feature with an emission maximum at 692 nm (Fig. 5b). Besides, the quantum yield is determined to be 23.8% under the excitation of 435 nm by a relative method (Fig. S2).

　　Based on the above structural and optical characterizations and analysis, the NIR emission of the NIR-CDs might derive from the molecular states. To further analyze the fluorescence mechanism of NIR-CDs, the UV-visible absorption and fluorescence emission of the sulfonated tetraphenylporphyrin were examined, as shown in Fig. S3. The sulfonated tetraphenylporphyrin aqueous solution shows typical peaks of the Soret band (411 nm) and Q-bands (515, 551, 582, and 637 nm). After hydrothermal carbonization, the Soret band peak (435 nm) of the resultant NIR-CDs' was significantly longer than that of sulfonated tetraphenylporphyrin (411 nm). Additionally,

the NIR-CDs show one absorption peak in the range of 500 to 800 nm, while sulfonated tetraphenylporphyrin has four Q-band absorption peaks. These changes indicate the aromatic rings of sulfonated tetraphenylporphyrin react and form larger conjugated structures. Fig. S3b shows typical fluorescence emission peaks of sulfonated tetraphenylporphyrin at 650 and 700 nm, respectively. The maximum emission peak of NIR-CDs is located at 692 nm, longer than the main fluorescence emission peak from sulfonated tetraphenylporphyrin (650 nm). The red-shift results from the extended conjugation of NIR-CDs, which reduces the energy gap between HOMO and LUMO[41]. To sum up, the NIR-CDs mainly present the molecular luminescence properties, but the UV absorption and fluorescence emission of NIR-CDs are red-shifted compared with that of sulfonated tetraphenylporphyrin, which might be due to the extended conjugation of NIR-CDs.

3.3 Cellular imaging

In view of the NIR-CDs' aqueous solubility and optical properties, the obtained NIR-CDs are expected to serve as potential near-infrared emission probes for bioimaging. The standard MTT assay was used to evaluate the cytotoxicity of NIR-CDs with Hela cells. NIR-CDs show negligible toxicity towards Hela cells even after incubation with NIR-CDs for 24 h at a relatively high concentration of 400 μg mL^{-1} (Fig. 6a). The Hela cells incubation with NIR-CDs were observed by a confocal fluorescence microscope under bright-field to evaluate the bio-imaging potential of the NIR-CDs. The excitation wavelength was set to be 543 nm. As shown in Fig. 6b, the NIR-CDs can quickly penetrate Hela cells, and produce brightly near-infrared emission at the position of the cytoplasm, indicating the NIR-CDs' excellent cell labeling ability. Near-infrared fluorescence imaging has attracted great attention due to its minimal damage to biological tissues, very low autofluorescence, deep penetration to tissue, and good spatial imaging ability. NIR-CDs as novel near-infrared probes show great potentials to be used in biological applications.

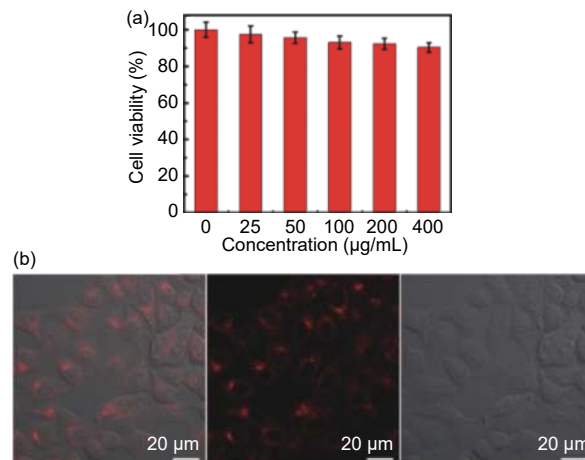## 4 Conclusion

In summary, the excitation-independent NIR-

Fig. 6 (a) Cell viability of HeLa cells after incubation with various concentrations of NIR-CDs; (b) Confocal images of Hela cells incubated with NIR-CDs at the concentration of 200 μg mL^{-1} obtained under dark field (right image), bright field (middle image) and their merged (left) image at the excitation of 543 nm laser.

CDs were synthesized via the solvothermal treatment of sulfonated tetraphenylporphyrin. The near-infrared fluorescence emission was mainly originated from the aggregated molecular states of CDs. The prepared NIR-CDs exhibit good dispersibility in water, a strong NIR emission at 692 nm, exceptional biocompatibility, minimal toxicity, and enhanced labelling capability in bio-imaging. The synergistic properties of the NIR-CDs assisted their remarkable application for near-infrared bio-imaging. Particularly, this study is a beginning step for the fabrication and bio-imaging application of NIR-CDs. Our laboratory is working on the multimodal imaging and therapy of NIR-CDs to expand their unique properties and potential applications.

Acknowledgements

References

［1］ Li L P, Lu C C, Li S J, et al. A high-yield and versatile method for the synthesis of carbon dots for bioimaging applications[J]. Journal of Materials Chemistry B, 2017, 5: 1935-1942.

［2］ Jia Q Y, Zhao Z Y, Liang K, et al. Recent advances and prospects of carbon dots in cancer nanotheranostics[J]. Materials Chemistry Frontiers, 2020, 4: 449-471.

［3］ Yang S T, Cao L, Luo P G, et al. Carbon dots for optical imaging in vivo[J]. Journal of the American Chemical Society, 2009, 131: 11308-11309.

［4］ Li J Y, Liu Y, Shu Q W, et al. One-pot hydrothermal synthesis of carbon dots with efficient up- and down-converted photoluminescence for the sensitive detection of morin in a dual-readout assay[J]. Langmuir, 2017, 33: 1043-1050.

［5］ Reyes D, Camacho M, Camacho M, et al. Laser ablated carbon nanodots for light emission[J]. Nanoscale Research Letters, 2016, 11: 424.

［6］ De Medeiros T V, Manioudakis J, Noun F, et al. Microwave-assisted synthesis of carbon dots and their applications[J]. Journal of Materials Chemistry C, 2019, 7: 7175-7195.

［7］ Liu M L, Xu Y H, NIU F, et al. Carbon quantum dots directly generated from electrochemical oxidation of graphite electrodes in alkaline alcohols and the applications for specific ferric ion detection and cell imaging[J]. Analyst, 2016, 141(9): 2657-2664.

［8］ Zhang X Y, Jiang M Y, Niu N, et al. Natural-product-derived carbon dots: from natural products to functional materials[J]. ChemSusChem, 2018, 11: 11-24.

［9］ Jiang K, Zhang L, Lu J, et al. Triple-mode emission of carbon dots: Applications for advanced anti-counterfeiting[J]. Angewandte Chemie International Edition, 2016, 55: 7231-7235.

［10］ Wu Z L, Zhang P, Gao M X, et al. One-pot hydrothermal synthesis of highly luminescent nitrogen-doped amphoteric carbon dots for bioimaging from Bombyx mori silk-natural proteins[J]. Journal of Materials Chemistry B, 2013, 1: 2868-2873.

［11］ Unnikrishnan B, Wu R S, Wei S C, et al. Fluorescent carbon dots for selective labelling of subcellular organelles[J]. ACS Omega, 2020, 5: 11248-11261.

［12］ Du J J, Xu N, Fan J L, et al. Carbon dots for in vivo bioimaging and theranostics[J]. Small, 2019, 15: 1805087.

［13］ Zhang J, Yu S H. Carbon dots: large-scale synthesis, sensing and bioimaging[J]. Materials Today, 2016, 19: 382-393.

［14］ Wang Q L, Huang X X, Long Y J, et al. Hollow luminescent carbon dots for drug delivery[J]. Carbon, 2013, 59: 192-199.

［15］ Sun S, Zhang L, Jiang K, et al. Toward high-efficient red emissive carbon dots: Facile preparation, unique properties, and applications as multifunctional theranostic agents[J]. Chemistry of Materials, 2016, 28: 8659-8668.

［16］ Li H X, Su D D, Gao H, et al. Design of red emissive carbon dots: Robust performance for analytical applications in pesticide monitoring[J]. Analytical Chemistry, 2020, 92: 3198-3205.

［17］ Gao W L, Song H H, Wang X, et al. Carbon dots with red emission for sensing of Pt^{2+}, Au^{3+}, and Pd^{2+} and their bioapplications in vitro and in vivo[J]. ACS Applied Materials & Interfaces, 2018, 10: 1147-1154.

［18］ Gao Y F, Jiao Y, Lu W J, et al. Carbon dots with red emission as a fluorescent and colourimeteric dual-readout probe for the detection of chromium(vi) and cysteine and its logic gate operation[J]. Journal of Materials Chemistry B, 2018, 6: 6099-6107.

［19］ Jiang K, Sun S, Zhang L, et al. Red, green, and blue luminescence by carbon dots: full-colour emission tuning and multicolour cellular imaging[J]. Angewandte Chemie International Edition, 2015, 54: 5360-5363.

［20］ Tan X Y, Li Y C, Li X H, et al. Electrochemical synthesis of small-sized red fluorescent graphene quantum dots as a bioimaging platform[J]. Chemical Communications, 2015, 51: 2544-2546.

［21］ Liu M L, Chen B B, Li C M, et al. Carbon dots: Synthesis, formation mechanism, fluorescence origin and sensing application[J]. Green Chemistry, 2019, 21: 449-471.

［22］ Li L P, Zhang R P, Lu C X, et al. In situ synthesis of NIR-light emitting carbon dots derived from spinach for bio-imaging applications[J]. Journal of Materials Chemistry B, 2017, 5: 7328-7334.

［23］ Pan L L, Sun S, Zhang L, et al. Near-infrared emissive carbon dots for two-photon fluorescence bioimaging[J]. Nanoscale, 2016, 8: 17350-17356.

［24］ Jiang K, Hu S Z, Wang Y C, et al. Photo-stimulated polychromatic room temperature phosphorescence of carbon dots[J]. Small, 2020, 16: 2001909.

［25］ Stobinski L, Lesiak B, Malolepszy A, et al. Graphene oxide and reduced graphene oxide studies by the XRD, TEM and electron spectroscopy methods[J]. Journal of Electron Spectroscopy and Related Phenomena, 2014, 195: 145-154.

［26］ Lei L, Wang W J, Wang C, et al. In situ growth of boron doped g-C_3N_4 on carbon fiber cloth as a recycled flexible film-photocatalyst[J]. Ceramics International, 2021, 47: 1258-1267.

［27］ Pan L L, Sun S, Zhang A D, et al. Truly fluorescent excitation-dependent carbon dots and their applications in multicolour cellular imaging and multidimensional sensing[J]. Advanced Materials, 2015, 27: 7782-7787.

［28］ Li W K, Feng J-T, Ma Z- Q. Nitrogen, sulfur, boron and flavonoid moiety co-incorporated carbon dots for sensitive fluorescence detection of pesticides[J]. Carbon, 2020, 161: 685-693.

［29］ Sun W, Meng X, Xu C, et al. Amorphous CoO_x coupled carbon dots as a spongy porous bifunctional catalyst for efficient photocatalytic water oxidation and CO_2 reduction[J]. Chinese Journal of Catalysis, 2020, 41: 1826-1836.

［30］ Ye Q H, Yan F Y, Luo Y M, et al. Formation of N, S-codoped fluorescent carbon dots from biomass and their application for the selective detection of mercury and iron ion[J]. Spectrochimica Acta Part A: Molecular and Biomolecular Spectroscopy, 2017, 173: 854-862.

［31］ Wang L, Li W T, Yin L Q. Full-colour fluorescent carbon quantum dots[J]. Science Advances, 2020, 6: eabb6772.

［32］ Ding K Q, Zhou L J, Qu R L. Honeycomb-shaped carbon particles prepared from bicycle waste tires for anodes in lithium ion batteries[J]. Materials Chemistry and Physics, 2020, 251: 123202.

［33］ Samantara A K, Chandra S S, Ghosh A. Sandwiched graphene with nitrogen, sulphur co-doped CQDs:An efficient metal-free material for energy storage and conversion applications[J]. Journal of Materials Chemistry A, 2015, 3: 16961-16970.

［34］ Palaniappan S, Amarnath C. A. Polyaniline-dodecylhydrogensulfate-acid salt: Synthesis and characterization[J]. Materials Chemistry and Physics, 2005, 92: 82-88.

［35］ Hoang V C, Nguyen L H., Gomes V G, et al. High efficiency supercapacitor derived from biomass based carbon dots and reduced graphene oxide composite[J]. Journal of Electroanalytical Chemistry, 2019, 832: 87-96.

［36］ Dager A, Uchida T, Maekawa T, et al. Synthesis and characterization of mono-disperse carbon quantum dots from fennel seeds: Photoluminescence analysis using machine learning[J]. Scientific Reports, 2019, 9: 14004.

［37］ Zhang J, Zhang X Y, Dong S S, et al. N-doped carbon quantum dots/TiO₂ hybrid composites with enhanced visible light driven photocatalytic activity toward dye wastewater degradation and mechanism insight[J]. Journal of Photochemistry and Photobiology A: Chemistry, 2016, 325: 104-110.

［38］ Li Y Y, Chen J J, Wang Y P, et al. Large-scale direct pyrolysis synthesis of excitation-independent carbon dots and analysis of ferric (III) ion sensing mechanism[J]. Applied Surface Science, 2021, 538: 148-151.

［39］ Liu T, Li N, Dong J X, et al. Fluorescence detection of mercury ions and cysteine based on magnesium and nitrogen co-doped carbon quantum dots and implicationlogic gate operation[J]. Sensors and Actuators B: Chemical, 2016, 231: 147-153.

［40］ Sun X C, BRüCKNER C, Lei Y. One-pot and ultrafast synthesis of nitrogen and phosphorus co-doped carbon dots possessing bright dual wavelength fluorescence emission[J]. Nanoscale, 2015, 7: 17278-17282.

［41］ Perepichka D, Bryce M. Molecules with exceptionally small HOMO-LOMO gaps[J]. Angewandte Chemie International Edition, 2005, 44(34): 5370-5373.

近红外荧光碳点的合成及其在生物成像中的应用

李利平[1,2]，　任晓烽[1]，　白佩蓉[2]，　刘　妍[2]，　许玮月[2]，　解　军[1,*]，　张瑞平[2,*]

（1. 山西医科大学 基础医学院，山西 太原 030001；

2. 山西医科大学 第三临床医学院，山西白求恩医院，山西 太原 030032）

摘　要： 由于红光/近红外发射具有深层组织穿透力强、自体荧光小、对生物组织损伤小等特点，具有上述特性的碳点的制备与生物成像应用备受关注。本文以磺化四苯基卟啉为前驱体，采用溶剂热法合成近红外发射的荧光碳点（NIR-CDs）。NIR-CDs 的最大发射峰位于 692 nm，其荧光发射具有激发波长非依赖性，经分析 NIR-CDs 的近红外荧光发射主要源于分子态发光。此外，NIR-CDs 还具有良好的水溶性和生物相容性、丰富的表面官能团、低毒性和优异的细胞标记能力，证实了 NIR-CDs 在细胞近红外成像中的应用潜力。本研究有望促进面向生物应用的近红外荧光碳点的发展，推动新型碳点的研究与实际应用。

关键词： 近红外荧光碳点；分子态发光；细胞标记；生物成像